Methods: SIMS was performed with a Cameca 7f-GEO using a 5 nA Cs^+ primary beam, collecting negative ions at high mass resolution (M/ΔM = 5500) to separate $^{16}OH^-$ from $^{17}O^-$ and $^{19}F^-$ from $^{18}OH^-$. Vacuum conditions (3 to 5 x 10^{-8} Pa) needed for ultra-low blank analyses (with detection limits for H_2O, F, and Cl as low as 1, 0.1, and 0.1 µg/g, respectively) were achieved using epoxy-free polishing and cleaning methods, pressing samples into indium, baking the instrument prior to analysis for 36 hours with sample mounts in the airlock, and a liquid N_2 cold trap. A 100 µm field aperture was used to collect ions from the central 8 µm of each analysis crater, eliminating contamination from crater edges. $^{12}C^-$ ion imaging and $^{12}C/^{18}O$ ratios were used to discriminate against organic contamination in cracks and surfaces (owing to sample preparation). After SIMS, we used high-resolution backscatter electron (BSE) imaging with a field-emission electron microprobe to identify sub-µm to µm-scale phases and micropores that are critical to our data interpretation.

The low detection limits in this study are illustrated in Figures 1 and 2.

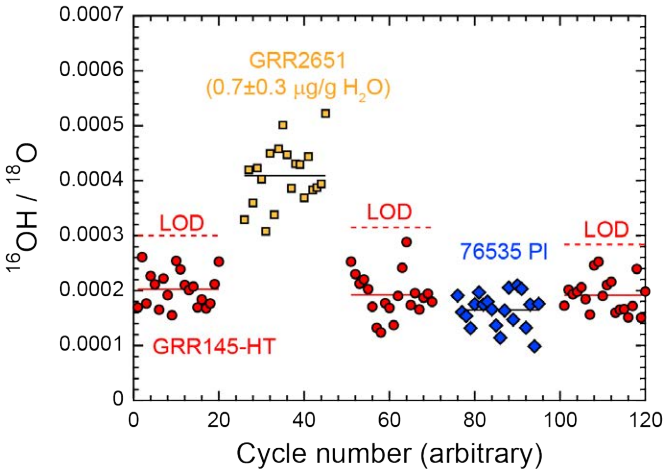

Fig. 1. Cycle-by-cycle $^{16}OH/^{18}O$ ratios for five sequential Pl analyses, demonstrating H detection limit. GRR2651 (0.7±0.3 µg/g H_2O; [5]) and 76535 (no detectable H) are bracketed by three analyses of the blank reference material GRR145-HT. Each analysis consists of 20 cycles through the mass sequence, with time spent for stage movement, pre-sputtering, and secondary beam tuning not reflected by the arbitrary, incremental cycle numbers on the x-axis. Solid lines represent average $^{16}OH/^{18}O$ for each analysis. Dashed lines represent the limit of detection (LOD) calculated from the mean and standard deviation of each respective block of 20 cycles on GRR145-HT.

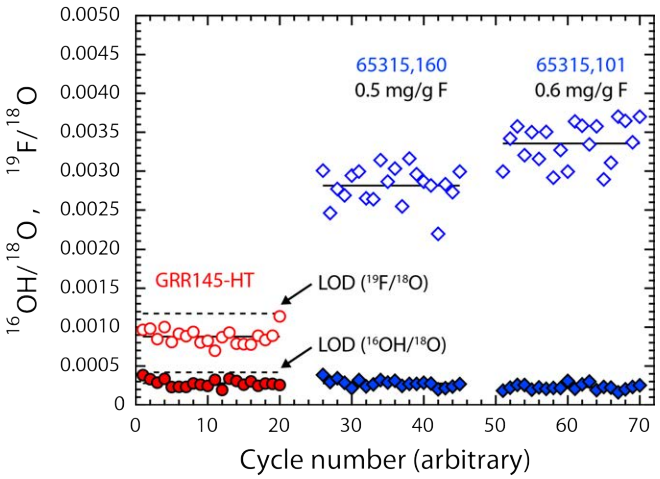

Fig. 2. Measurement of blank (dehydrated Pl, GRR145-HT) followed by two measurements on different Pl crystals extracted from FAN 65315, demonstrating F significantly above LOD but OH below LOD. Open symbols are $^{19}F/^{18}O$ measurements, closed symbols are $^{16}OH/^{18}O$. Solid lines are the mean of each measurement, dashed lines are LOD.

Micropores in olivine and plagioclase:

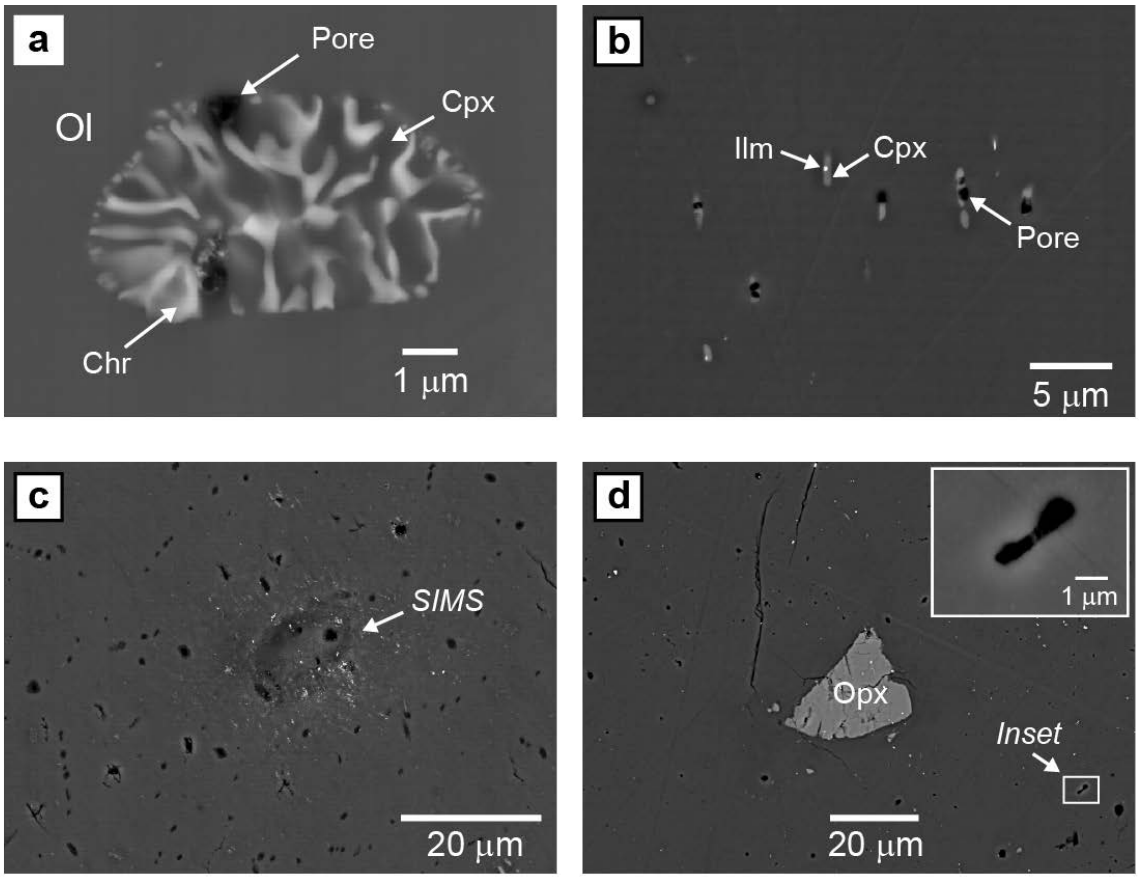

Fig. 3. Examples of micropores imaged with BSE. **a.** Symplectite inclusion in olivine from mare basalt 14072. The edges of these symplectites – consisting of chromite, clinopyroxene, and micropores – are crystallographically aligned with the olivine, implying exsolution during cooling. **b.** Crystallographically aligned inclusions (clinopyroxene ± ilmenite ± micropore) in plagioclase from troctolite 76535, also likely formed by exsolution during static cooling. **c.** Micropores in plagioclase in an Mg-suite clast from 73255, inferred to be vapor-filled inclusions associated with shock metamorphism. The SIMS analysis crater clearly intersects some micropores; the analysis yielded 1.9 μg/g H_2O and 3.4 μg/g F. **d.** Heavily shocked sample 60015. The orthopyroxene crystal in the image is relatively unshocked, but elsewhere in the sample this phase has been partially shock-melted. Sample contains numerous micropores. Inset shows a magnified view of a micropore with an arcuate shape similar to vapor bubbles in melt inclusions imaged in thin section by [8].

Partitioning: Using an F partition coefficient between Pl and melt of 0.02 [9], we estimate 50 μg/g F in the melt and back-calculate to a value of 15 μg/g F in the LMO using a simple fractional crystallization model and a bulk partition coefficient from [10]. This value is within the range of previous estimates for F in the bulk silicate Moon [1,2].

References: [1] McCubbin F.M. et al. (2015) *Am. Mineral.* **100**, 1668–1707 [2] Hauri E.H. et al. (2015) *EPSL* **409**, 252-264 [3] Mosenfelder J.L. et al. (2011) Am. Mineral. **96**, 1725-1741 [4] Mosenfelder J.L. and Rossman G.R. (2013) *Am. Mineral.* **98**, 1026-1041 [5] Mosenfelder J.L. and Rossman G.R. (2013) *Am. Mineral.* **98**, 1042-1054 [6] Mosenfelder J.L. et al. (2015) *Am. Mineral.* **100***,* 1209-1221 [7] Hui H. et al. (2013) *Nat. Geosci.,* **6**, 177–180.
References: [8] Sclar C.B. and Bauer J.F. (1974) *Proc. Lunar Sci. Conf.* **5**, 319-336 [9] Caseres J. et al. (2017) *LPS XXXXVIII.* Abstract #2303 [10] Rosenthal A. et al. (2015) *EPSL,* **412**, 77-87.